On the Use of Supported Ceria Membranes for Oxyfuel process / Syngas Production

M. Pilar Lobera[1], José M. Serra[1]*, Søren P. Foghmoes[2], Martin Søgaard[2], Andreas Kaiser[2]

[1]Instituto de Tecnología Química (Universidad Politécnica de Valencia - Consejo Superior de Investigaciones Científicas), Av. Naranjos s/n, E-46022 Valencia, Spain.

[2]Fuel Cells and Solid State Chemistry Department, Risø National Laboratory for Sustainable Energy, Technical University of Denmark - DTU, Building 228, P.O. Box 49, DK-4000 Roskilde, Denmark

** Corresponding author. Tel: + 34.963879448 E-mail: jmserra@itq.upv.es*

Journal of Membrane Science 385– 386 (2011) 154– 161 (doi: 10.1016/j.memsci.2011.09.031)

Abstract

Ceramic oxygen transport membranes (OTMs) enable selective oxygen separation from air at high temperatures. Among several potential applications for OTMs, the use in (1) oxygen production for oxyfuel power plants and (2) the integration in high-temperature catalytic membrane reactors for alkane upgrading through selective oxidative reactions are of special interest. Nevertheless, these applications involve the direct contact of the membrane surface with carbon-rich atmospheres. Most state-of-the-art permeable membranes are based on perovskites, which are prone to carbonation under operation in CO_2-rich environments and/or decomposition in reducing gas environments. The oxygen flux through supported thin film membranes of $Ce_{0.9}Gd_{0.1}O_{1.95-\delta}$ (CGO) with 2% mol. of cobalt was measured for oxygen separation in oxyfuel processes and in syngas production and degradation was compared to perovskite membranes. The CGO membranes consist of a 27 μm-thick gastight CGO layer supported on a porous CGO substrate. The flat surface of the membrane was coated using two different porous catalytic layers aiming to improve the oxygen activation rate on the permeate side while the porous substrate was infiltrated with an oxygen reduction catalyst. Oxygen separation was studied using air as feed and argon/CO_2 or argon/CH_4 mixtures as sweep gas in the temperature range 750-1000 ºC. The supported membrane exhibited a maximum oxygen flux of ca. 5 $ml \cdot min^{-1} \cdot cm^{-2}$ at 1000 ºC when diluted methane was used as sweep gas. The CGO membrane showed high stability in CO_2 (in contrast to tests on $La_{0.6}Sr_{0.4}Co_{0.2}Fe_{0.8}O_{3-\delta}$ (LSCF) membranes) and no detrimental effect on the oxygen flux is observed when CO_2 is present in the sweep gas even at temperatures below 800 ºC. Moreover, the SEM analysis showed that membrane integrity remained stable after the permeation tests using CO_2.

Keywords: *cerium gadolinium oxide, supported membrane, tape casting, MIEC; syngas; oxyfuel*

1. Introduction

Ceramic mixed ionic-electronic conducting (MIEC) membranes enable the selective oxygen separation from air at high temperatures. Two key industrial applications of oxygen-transport membranes are (1) oxygen production for power generation from fossil fuel in oxyfuel power plants [1, 2] and (2) the integration in high-temperature catalytic membrane reactors for methane or alkane upgrading by selective oxidative conversions, for instance, partial oxidation of methane (POM) to produce syngas [3, 4]. However, these applications involve the contact with carbon-bearing atmospheres and most of state-of-the-art highly-permeable MIEC membranes do not tolerate the operation under CO_2-rich environments, due to carbonation processes [5-7]. The most promising materials are perovskites with the formula ABO_3 [8], comprising alkali-earth metal cations in the *A*-position. High oxygen permeation fluxes have been reported even in oxidizing conditions, for single phase materials such as $SrCo_{0.8}Fe_{0.2}O_{3-\delta}$ (SCF) [9], $Ba_{0.5}Sr_{0.5}Co_{0.8}Fe_{0.2}O_{3-\delta}$ (BSCF) [10, 11], $La_{0.6}Sr_{0.4}Co_{0.2}Fe_{0.8}O_{3-\delta}$ (LSCF) [12]. However, these perovskites are chemically unstable under large oxygen chemical potential gradients (e.g. air/methane) and in presence of CO_2, SO_2 or H_2O, leading to degradation in oxygen flux and possibly mechanical integrity with time [6, 7, 13].

Lanthanide substituted ceria materials present a combination of high oxygen-ion mobility and chemical compatibility with water and carbon dioxide at high temperatures. *n*-type electronic conductivity can be introduced into the structure by partial reduction of the cerium (IV) ion at high temperatures under reducing conditions. Recent reports show the potential of oxygen separation in monolithic doped/multidoped ceria membranes [14-16]. Moreover, gadolinium doped ceria ($Ce_{0.9}Gd_{0.1}O_{1.95-\delta}$, CGO) was suggested as oxygen separation membrane for syngas application. On planar, thin film CGO membranes on porous NiO-YSZ supports oxygen fluxes as high as 16 ml min^{-1} cm^2 could be obtained by placing the membrane between air and humidified hydrogen (or methane) at 900°C [17, 18].

The present work shows the functional characterization of oxygen separation membranes made of a gastight thin film layer of $Ce_{0.9}Gd_{0.1}O_{1.95-\delta}$ (CGO), supported on a porous CGO substrate. The top flat surface of the membrane was coated using two different porous catalytic layers aiming to improve the oxygen activation rate on the permeate side. Oxygen separation was studied using air as feed and argon/CO_2 or

argon/CH_4 mixtures as sweep gas in the temperature range 750-1000 ºC. Special attention is paid to the membrane stability in CO_2 under operation.

2. Experimental

A thin film CGO membrane supported by a porous CGO substrate was prepared using tape casting, lamination, co-sintering and cutting. The ethanol based slurries for tape casting of the support and membrane layer were prepared by ball milling an ultra low surface area powder of CGO from Rhodia S.A. (France), a PVB based binder system and a polyethylene imine (PEI, branched, M.W. 10,000, 99% Alfa Aesar) as a dispersant. 2 mol% of cobalt(II) nitrate (Cobalt(II) nitrate hexahydrate, 97.7 % min, Alfa Aesar) was added as a sintering aid after drying in a desiccator to remove excess water. In the slurry for tape casting of the porous CGO substrate about 5 vol.-% graphite (V-UF1, 99.9, Graphit Kropfmühl AG, Germany) was added as a pore former. The tape casted layers of the thin film CGO membrane and the porous CGO support were combined by lamination (i.e., application of heat and pressure on to the tubes between two rolls). Round membranes (Ø = 34 mm) were stamped out from the green membrane tapes before sintering. In a binder removal step the organics were removed by a very slow de-bindering profile to avoid damage of the structure. Subsequently, the structure was sintered in air at 1300 ºC for 2 h. The sintered membrane structures were laser-cut to the final dimensions (diameter of 15 mm, total thickness of about 0.3 mm and a CGO membrane thickness of about 25 μm). After sintering, the porous supports of CGO were impregnated with nitrates corresponding to the nominal composition $La_{0.6}Sr_{0.4}Co_{1.05}O_{3-\delta}$ (LSC40). In a previous study it has been shown that LSC40 impregnated in a very porous (>70%) and thin (25 μm) backbone structure provided a highly active oxygen reduction electrode/activation layer [19]. In that case it was found that an optimal performance was found if LSC40 was impregnated in an amount corresponding to 17 vol% in the CGO backbone. The impregnation for the supports characterized here was carried out in a similar way as by *Samson et al. [19]*, except that the cells between each impregnation were inserted directly into a furnace at 350°C.

On top of the CGO membrane layer, a porous catalytic layer was applied by screen-printing. The catalyst layers were composed of either $Ba_{0.5}Sr_{0.5}Co_{0.8}Fe_{0.2}O_{3-\delta}$ (BSCF) or

cobalt-doped $Ce_{0.8}Tb_{0.2}O_{2-\delta}$ (CeTbO+Co). BSCF powder was provided by Fraunhofer IKTS (Hermsdorf, Germany) and cobalt-doped $Ce_{0.8}Tb_{0.2}O_{2-\delta}$ (CeTbO+Co) was prepared by a co-precipitation route following the procedure described in ref. [14]. Formation of the corresponding crystalline structure (perovskite or fluorite) was checked by X-ray diffraction, using a Philips X'pert Pro equipped with X'celerator detector using monochromatic Cu Kα radiation. XRD patterns were recorded in the 2θ range from 10 to 90 º and analyzed using X'pert Highscore Plus software (PANalytical). The screen-printing inks were prepared by mixing the ball-milled powders with a solution of 94 wt.% terpineol and 6 wt.% ethylene cellulose. Graphite (Aldrich) was added as a pore former in the screen-printing ink. Then, graphite is removed in the ulterior sintering step. This process generates a macroporous system that aims to promote the gas transport through the catalytic layer. The ink homogenization was conducted using a three-roll mill. The coated membranes were sintered in air for 2 h. The sintering temperature of the screen printed layers results from the diverse sintering activities of each material, thereby the membrane with a BSCF coating was sintered at 1010 ºC and the membrane with a CeTbO+Co coating, at 1050 ºC. The material CeTbO+Co has been chosen for the following reasons [14]: (1) stability in CO_2-bearing atmospheres; (2) mixed ionic-electronic conductivity at high pO_2 and high temperatures; and (3) high surface exchange activity as determined by conductivity relaxation. Figure 1 shows a schematic cross section of the membrane assembly and details of the testing setup. The microstructure of the membranes was analyzed by SEM and EDS in a JEOL JSM6300 electron microscope.

$La_{0.6}Sr_{0.4}Fe_{0.8}Co_{0.2}O_{3-\delta}$ (LSCF) monolithic membranes were prepared as reference by uniaxial pressing followed by sintering at 1250 ºC. The final membrane dimensions were 15 mm in diameter and ~ 0.8 mm thickness. After sintering the membrane surface was polished prior to testing.

Oxygen permeation tests were performed on 15 mm diameter disk-shape membranes. Sealing was done using gold gaskets in a quartz lab-scale reactor described previously [5]. The temperature was measured by a thermocouple close to the membrane surface. Oxygen was separated from a synthetic air mixture (21% v/v O_2). The permeate was analyzed by on-line gas chromatography using a micro-GC (Varian CP-4900) equipped with Molsieve5A, Pora-Plot-Q glass capillary, and CP-Sil modules. All streams were

individually mass flow controlled. Membrane gas leak free conditions were ensured by monitoring nitrogen concentration on the permeate gas stream.

3. Results and Discussion

3.1 Membrane microstructure

Figure 2 presents the SEM images of fracture cross-section of the samples after permeation tests. Figure 2a shows an overview of the CGO porous support (thickness of support is approximately 300 µm). The porosity of the support is about 25% determined by Hg porosimetry. The pore size of the substrates ranges from 1 to 4 µm while the CGO grain size in the support is 0.5 to 1 µm. Regarding the catalytic substrate infiltration, EDS analysis over larger areas indicated that it was only feasible to impregnate 1-2 Vol% of LSC40 in the porous support structure after 6 impregnations. The low amount impregnated in the present porous structure is attributed to the relatively low porosity and small pore size. This can pose a problem as there is not enough oxygen reduction catalyst material in the structure and therefore a large part of the driving force for the oxygen transport can in a worst case scenario be located at the feed side of the membrane. Further ceramic processing development on CGO membranes (not reported in this paper) indicates that the porosity in the support can be adjusted to 35 to 45% by the amount of pore former (graphite) and the sintering conditions.

The thickness of the gastight CGO membrane was determined to be 27 ± 0.5 µm from SEM images (see Figure 2b). Figure 2c and 2d show the membrane with different catalytic layers composed of BSCF and CeTbO+Co, respectively. The oxygen BSCF activation layer have an open microstructure with macropores and a homogeneous thickness of 19 ± 0.5 µm. The CeTbO+Co catalytic layer presents a larger thickness of 54 ± 0.5 µm and the mean pore size in this case is significantly smaller due to the lower sintering activity of CeTbO+Co. Both layers show an average particle size well below 1 µm while the mean size of the primary CeTbO+Co crystallites is 60 nm as determined by XRD. Finally, the integrity of both catalytic porous layers was preserved during the whole oxygen permeation tests, as inferred by XRD and SEM analysis.

3.2 Oxygen permeability

3.2.1 *Influence of sweep gas flow rates, Q_{Sweep}*

Figure 3 shows the oxygen permeation fluxes through the surface-activated CGO supported membranes at various flow rates of Ar as sweep gas (Q_{Sweep}). The $J(O_2)$ was strongly influenced by the increase of the sweep gas flow rate; and this is attributed to two main effects. Firstly, the decrease in the oxygen partial pressure in the permeate side (pO_2'') and the consequent increase in the oxygen chemical potential gradient across the thickness of the membrane (i.e. the driving force of the oxygen permeation process). Secondly, the variation of the sweep gas flow rate also affects the fluid dynamics behavior of the membrane reactor (Figure 1b) due to an increase in the sweep gas flow rate reduces the concentration polarization resistance at the permeate membrane side. Concentration polarization becomes typically more relevant in this kind of setup [20] for gas flow rates below 100 $ml \cdot min^{-1}$ and this is probably the reason for the steep change at 50 $ml \cdot min^{-1}$ in Figure 3, which is more visible for the membrane reaching the highest flux values. Consequently, gas-phase resistance appears to be a minor contribution to the whole process resistance, especially at low $J(O_2)$ values and when compared to that of solid state diffusion and exchange reactions [10, 20]. On the other hand, proper gas sweeping allows decreasing the permeate partial pressure just by a simple dilution process.

The permeation flux obtained using the membranes with two different activation layers differ substantially. Namely, the BSCF-activated layer allows achieving an oxygen flux around 4 times higher than the flux obtained using the CeTbO-activated membranes. The main reasons for this are related to characteristics of the CeTbO+Co porous layer:

(1) The ambipolar conductivity of the CeTbO+Co material under high pO_2 is very limited especially regarding BSCF and therefore the expected catalytically active thickness of the porous layer may be very small. Additionally, the CeTbO+Co layer presents a larger thickness (54 μm, almost a 3 times of the BSCF layer). Both effects would lead to (a) the reduction of the catalytically-active thickness of the porous layer and (b) possible concentration polarization in the gas transport through the pore system. In summary, it seems that the CeTbO layer adds a new

resistance in the permeation process (at high pO_2 in the sweep) instead of improving the surface exchange process.

(2) The catalytic activity, i.e. surface exchange rate in this case, is smaller than the one exhibited by BSCF and this may result in a lower permeation flux, although surface exchange seems not to be a major limiting step under the current operating conditions, as suggested below.

The oxygen flux ($J(O_2)$) through a MIEC membrane can be increased by reducing the thickness of the membrane, until its thickness becomes less than a characteristic value, L_c* ($L/L_c<<1$), at which point the flux of oxygen is under conditions of mixed control of the surface exchange kinetics and bulk diffusion. A generalized Wagner equation† has been proposed to describe the oxygen flux within this regime, where the surface-exchange reactions are assumed as sequential steps: adsorption from the gas phase, charge transfer reaction between the adsorbed species and the bulk including the reverse reactions. The oxygen permeation flux has been described successfully for perovskite-based membranes [23, 24] by the following empiric equation

$$J(O_2) = \frac{\sigma_i^o RT}{16nLF^2}(pO_2'^n - pO_2''^n) \qquad (1)$$

From the value n the rate-limiting step of the oxygen permeation can be identified. For $n < 0$, bulk diffusion of the oxygen ions is the rate-limiting step and ($J_{O2} \propto \ln pO_2'/pO_2''$); while for $n > 0.5$, the rate-controlling step is the reaction of molecular oxygen with the membrane surface. For $0 < n < 0.5$, the $J(O_2)$ is influenced by both surface reaction and bulk diffusion.

---

* The characteristic length in highly electronic mixed conductors, L_c, is defined as the ratio of the bulk diffusion coefficient to the surface exchange coefficient of the membrane ($L_c = D/k$). However, this value has to be redefined for membrane materials limited by the electronic conductivity and whose ambipolar conductivity varies dramatically as a function of pO_2.

† $$J(O_2) = \frac{RT}{16LF^2}\int_{pO_2''}^{pO_2'} \sigma_{amb}(pO_2)\, d\ln pO_2$$

where $J(O_2)$ is the oxygen permeation rate, R gas constant, F Faraday constant, L membrane thickness, pO_2' and pO_2'' the oxygen partial pressure at the high pressure side and the low pressure side, adfespectively. σ_{amb} (S m^{-1}) is the average ambipolar conductivity (σ_{amb} =10^{-2} S m^{-1}, at 700 ºC) [21, 22]

A linearized plot of equation (1) with *n* as a fit parameter is shown in Figure 4 for 950 ºC and 850 ºC. The experimentally determined coefficients for the BSCF coating at 950 ºC and 850 ºC are 0.0074 and 0.0086 respectively. In the case of the CeTbO+Co coating, *n* had a value of 0.022 and 0.016 for the experiments performed at 850 ºC and at 950 ºC. These results may indicate that the oxygen flux through the CGO supported membrane is controlled by both vacancy diffusion and interface exchange reactions. However, the values for the fit parameter are close to zero, indicating that the bulk transport is more important than the surface exchange reactions. In Figure 4a, the two data points corresponding to the lowest sweep flow rate slightly deviate from the model (eq. 1) and this is ascribed to the effect of small limitations in the gaseous transport [20], which leads to pO_2 gradients in the permeate chamber and an increased local pO_2 on the membrane surface.

3.2.2 Influence of porous support

For the asymmetric membranes, the porous structure should have low gas transport resistance so that the diffusion of gas in the support does not determine the permeation rate. In the support pores, the main transport mechanism is the molecular gas diffusion, thus the structure of the pore system is essential in the oxygen permeability. The influence of the porous support can be evaluated by means of the change of pO_2 in the feed side or modifying the fluid dynamic in the feed reactor compartment (i.e., different feed flow rates). In a first approach, the influence of the support in the permeation process was evaluated, when the feed gas is switched from air (pO_2'=0.21 atm) to pure oxygen (pO_2'=1 atm), as a result only a slight increase in the oxygen permeation flux is observed due to the fact that the support has a proper microstructure (Figure 5). An opposite case has recently been reported for BSCF asymmetric membranes [10], where the porous support had a negative effect on the oxygen flux because it produces a concentration polarization on the air side. In that case, the obtained oxygen fluxes exceeded values of 12 $ml \cdot min^{-1} \cdot cm^{-2}$ in air and therefore the pore system of the ceramic substrate limited the gas diffusion and caused the accumulation of nitrogen in the pores. In the present case, when pure oxygen is used as feed gas, the subtle increase in oxygen flux may be partially related to the slight rise in the driving force. Calculating with the Nernst equation [25] (as done frequently in solid oxide fuel cell research) the theoretical

increase in the driving force is from 0.224 V to 0.262 V at 850 ºC and, considering the empiric expression for the driving force (equation-1 and Figure 4), the driving force expressed in (pO_2'^{n}-pO_2"^{n}) increases from 0.055 to 0.083 at 850 ºC when pure oxygen is used as feed gas instead of synthetic air.

Figure 6 shows the oxygen permeation flux through CGO supported membranes as a function of temperature and feed flow rate. In both cases, a rise in the Q_{Feed} leads to a slight increase in the $J(O_2)$ reached. This is ascribed to an improvement of the fluid dynamics conditions in the feed reactor compartment (i.e., a lower gas concentration polarization effect at the feed side) and a better gas diffusion in the support pores. Concentration polarization due to non-optimized fluid dynamics is more important when high $J(O_2)$ are reached (Figure 6a), e.g. at high temperatures and BSCF-coated membrane. Therefore, the variation in the Q_{Feed} affects to a lesser extent at lower $J(O_2)$.

3.2.3 Oxygen permeation using methane as sweep gas

CGO is a good oxygen ionic conductor but possesses a low electronic conductivity, especially at the more oxidizing conditions, limiting oxygen transport. Under more reducing atmosphere the mixed conductivity (electronic conductivity) of CGO increases substantially and allows higher oxygen fluxes. Figure 7 shows the oxygen flux through CGO supported membranes obtained using as sweep gas (1) diluted methane (15% in Ar) or (2) argon (oxidizing conditions). A CeTbO+Co activated membrane was used due to its higher stability in reducing conditions and in carbon-bearing atmospheres. This experiment demonstrates the applicability of CGO supported membranes in the partial oxidation of methane and other hydrocarbons into syngas or upgraded molecules, such as olefins and aromatics. The use of methane sweep (reducing conditions) enables the ~15-fold increase in oxygen flux. This increase is ascribed to (1) to the partial reduction of Ce (IV) to Ce(III), which results in the substantial increase in the (n-type) electronic conductivity, and therefore augmenting the ambipolar conductivity; and (2) the increase in the separation driving force, i.e., the theoretical[‡] chemical gradient across the membrane, .e.g. from 0.224 V to 1.20 V at 850ºC.

[‡] Neglecting concentration polarization issues

3.3 Oxy-fuel processes

Oxyfuel combustion in fossil fuel power plants involves the use of pure oxygen instead of air as oxidizing agent. A preferred oxyfuel process design utilizes part of the exhaust (flue) gases as sweep stream in the membrane module. The final exhaust is principally made of water, around 1-2% O_2 and CO_2, which can readily be separated, transported and stored (CCS strategies). In this oxyfuel operation concept, the membrane has direct contact with the flue gas which can contain a number of chemically aggressive impurities such as CO_2, SO_2, Cl_2, HCl, HF and NO_2. The membrane has to tolerate these and still have an adequate flux of oxygen, although the separation driving force is reduced to the remaining oxygen in the recycle flue gas. Hence, the OTMs in oxyfuel have to satisfy the strong requirements regarding chemical stability at elevated temperatures. As BSCF decomposes dramatically in CO_2 atmospheres in the temperature range studied the chemical stability, towards CO_2, of the CGO supported membrane coated with a CeTbO+Co activation layer was analyzed. The membrane was exposed to (1) a mixture of 15 % CO_2 and Ar and (2) a mixture of 1 % O_2 and Ar on the sweep gas inlet.

In order to study the poisoning effect of CO_2, the coated CGO supported membrane was exposed to a stream of 15 % CO_2 in argon on the sweep side. This condition was maintained 48 h at 750 ºC. Then, the sweep gas was switched to a pure Ar feed and the evolution of the $J(O_2)$ as a function of the temperature was studied in two consecutive steps (see figure S3 in supporting material illustrating the experimental procedure).

In a first step, the temperature was increased during the oxygen permeation tests (from 750 ºC to 1000 ºC), and then, in a consecutive phase, these tests were repeated while the temperature was decreased (Figure 8). For comparison, this experimental procedure was carried out using a monolithic LSCF thick membrane (thickness ~ 0.8 mm). For the LSCF membrane (Figure 8a), a lowering of $J(O_2)$ was observed at lower temperatures due to a degradation of the membrane surface. However, as the temperature was raised, the carbonates deposited on the membrane surface decomposed which gives rise to the observed hysteresis. This behavior was not observed for the coated supported CGO membrane. Surface carbonates species do apparently not form on the CGO surface while they do on the LSCF surface at lower temperatures. However, postmortem inspection of the LSCF membrane by SEM analysis showed that the surface exposed to

the sweep gas does not show degradation or changes in the surface morphology (See fracture cross-section of the LSCF membrane in Fig. S4 in supporting material).

Figure 9 shows the oxygen permeation flux through the monolithic LSFC and the CGO supported membrane as a function of the temperature when the permeated side was exposed at different sweep gas: (1) argon and (2) 15 % CO_2 in argon. The experiments were performed decreasing the temperature from 1000 ºC to 750 ºC. Figure 9a suggests that the operation of the LSCF membrane is slightly affected by the surface exchange in the sweep side, especially at lower temperatures, since typically the presence of CO_2 reversibly reduces the exchange rate. For the monolithic LSCF membrane, the impacto of CO_2 on the oxygen flux becomes more important when decreasing the temperature. This is attributed to the formation of carbonates on the surface that reduce the catalytic activity (surface exchange) of the membrane surface on the permeate side. On the other hand, the CGO supported membrane is not influenced by the presence of CO_2. As the operation of this membrane is principally governed by bulk transport, it can only be concluded that surface exchange is not limiting the permeation process even under CO_2, which constitutes an indication of the high stability of the ceria surface at work.

Another important component of the flue gas besides CO_2 is O_2 which comes from the oxygen excess necessary for combustion. The oxygen excess ratio has a significant influence on the oxygen permeation process, since it reduces dramatically the separation driving force. As shown in Figure 10, a lower $J(O_2)$ was obtained when the experiment was carried out using a mixture of O_2 (1%) and argon as sweep gas. The decrease in the driving force, i.e. lower partial pressure gradient (from 0.224 to 0.129 V at 850 ºC), leads to a reduction in the oxygen flux of ~ 50% and this flux decrease becomes more important with decreasing temperatures and it is more visible for the BSCF-coated membrane. These results demonstrate that supported CGO membranes can be operated using a limited oxygen gradient but the oxygen flux is reduced to below 1 $ml \cdot min^{-1} \cdot cm^{-2}$. The lower flux is due to the small p-type electronic conductivity, which controls the permeation process under these operating conditions.

4. Conclusions

The functional characterization of oxygen separation membranes based on $Ce_{0.1}Gd_{0.9}O_{1.95-\delta}$ (with 2% mol. of cobalt) has been carried out. The asymmetric membranes are made of a 27 μm-thick gastight layer supported on a porous CGO substrate. Furthermore, the top gastight surface of the membrane was coated using two different porous catalytic layers aiming to improve the oxygen activation rate in the permeate side while the porous substrate was infiltrated with LSC. Oxygen separation was studied using air as feed and argon/CO_2 or argon/CH_4 mixtures as sweep gas in the temperature range 750-1000 ºC. The main conclusions of this study are:

- The use of a reducing atmosphere (15 % CH_4 in Ar) allows a very strong improvement in the oxygen permeation flux (by a factor of ~ 100), due to the improvement of the ambipolar conductivity and the increase in the separation driving force.

- These results demonstrate the possibility of industrial application of these membranes in oxyfuel operation conditions and in the production of syngas, by combining CO_2 resistance with either (1) O_2 permeability with small O_2 gradients in oxidizing conditions; or (2) chemical and structural stability in reducing conditions.

- Oxygen permeation flux of thin film CGO membrane with a CeTbO+Co coating remained stable after treatment at 750 ºC in CO_2 for 48 hours. The integrity of the membrane assembly was also confirmed by SEM and XRD after the permeation study. Further work might be required to investigate the effect of other poisoning compounds typically present in flue gases (such as H_2S or SO_2) on the membrane stability.

Acknowledgements

Financial support by the Spanish Ministry for Science and Innovation (Project ENE2008-06302) and by the EU through FP7 NASA-OTM Project (NMP3-SL-2009-228701) is kindly acknowledged.

References

[1] R. Bredesen, K. Jordal, O. Bolland, High-temperature membranes in power generation with CO_2 capture. Chemical Engineering and Processing, 43 (2004) 1129-1158.

[2] H. Stadler, F. Beggel, M. Habermehl, B. Persigehl, R. Kneer, M. Modigell, P. Jeschke, Oxyfuel coal combustion by efficient integration of oxygen transport membranes. International Journal of Greenhouse Gas Control, 5 (2011) 7-15.

[3] J. Caro, T. Schiestel, S. Werth, H. Wang, A. Kleinert, P. Kölsch, Perovskite hollow fibre membranes in the partial oxidation of methane to synthesis gas in a membrane reactor. Desalination, 199 (2006) 415-417.

[4] H.Q. Jiang, H.H. Wang, S. Werth, T. Schiestel, J. Caro, Simultaneous Production of Hydrogen and Synthesis Gas by Combining Water Splitting with Partial Oxidation of Methane in a Hollow-Fiber Membrane Reactor. Angewandte Chemie-International Edition, 47 (2008) 9341-9344.

[5] M.P. Lobera, S. Valero, J.M. Serra, S. Escolástico, E. Argente, V. Botti, Optimization of ODHE membrane reactor based on mixed ionic electronic conductor using soft computing techniques. Chemical Engineering Science, In Press, Corrected Proof (2010); doi:10.1016/j.ces.2010.12.013.

[6] M. Arnold, H. Wang, A. Feldhoff, Influence of CO_2 on the oxygen permeation performance and the microstructure of perovskite-type $(Ba_{0.5}Sr_{0.5})(Co_{0.8}Fe_{0.2})O_{3-\delta}$ membranes. Journal of Membrane Science, 293 (2007) 44-52.

[7] V.V. Kharton, A.V. Kovalevsky, A.P. Viskup, A.L. Shaula, F.M. Figueiredo, E.N. Naumovich, F.M.B. Marques, Oxygen transport in $Ce_{0.8}Gd_{0.2}O_{2-\delta}$-based composite membranes. Solid State Ionics, 160 (2003) 247-258.

[8] J. Sunarso, S. Baumann, J.M. Serra, W.A. Meulenberg, S. Liu, Y.S. Lin, J.C. Diniz da Costa, Mixed ionic-electronic conducting (MIEC) ceramic-based membranes for oxygen separation. Journal of Membrane Science, 320 (2008) 13-41.

[9] J. Vente, S. McIntosh, W. Haije, H. Bouwmeester, Properties and performance of $Ba_xSr_{1-x}Co_{0.8}Fe_{0.2}O_{3-\delta}$ materials for oxygen transport membranes. Journal of Solid State Electrochemistry, 10 (2006) 581-588.

[10] S. Baumann, J.M. Serra, M.P. Lobera, S. Escolástico, F. Schulze-Küppers, W.A. Meulenberg, Ultrahigh Oxygen Permeation Flux Through Supported $Ba_{0.5}Sr_{0.5}Co_{0.8}Fe_{0.2}O_{3-\delta}$ Membranes. Journal of Membrane Science, 377 (2011) 195-205.

[11] A. Leo, S. Smart, S. Liu, J.C. Diniz da Costa, High performance perovskite hollow fibres for oxygen separation. Journal of Membrane Science, 368 (2011) 64-68.

[12] O. Büchler, J.M. Serra, W.A. Meulenberg, D. Sebold, H.P. Buchkremer, Preparation and properties of thin $La_{1-x}Sr_xCo_{1-y}Fe_yO_{3-\delta}$ perovskitic membranes supported on tailored ceramic substrates. Solid State Ionics, 178 (2007) 91-99.

[13] H.J.M. Bouwmeester, A.J. Burggraaf, A.J. Burggraaf, L. Cot, Chapter 10 Dense ceramic membranes for oxygen separation, in: Membrane Science and Technology, Elsevier, 1996, pp. 435-528.

[14] M. Balaguer, C. Solís, J.M. Serra, Study of the transport properties of mixed ionic electronic conductor $Ce_{1-x}Tb_xO_{2-\delta}$ + Co (x=0.1,0.2) and evaluation as oxygen transport membrane. Chemistry of Materials, 23 (2011) 2333-2343.

[15] B.T. Dalslet, Measurement and modeling of the defect chemistry and transport properties of ceramic mixed ionic and electronic conductors, in: University of Twente, University of Twente, Twente, 2008.

[16] D.P. Fagg, A.L. Shaula, V.V. Kharton, J.R. Frade, High oxygen permeability in fluorite-type $Ce_{0.8}Pr_{0.2}O_{2-\delta}$ via the use of sintering aids. Journal of Membrane Science, 299 (2007) 1-7.

[17] A. Kaiser, S. Foghmoes, C. Chatzichristodoulou, M. Søgaard, J.A. Glasscock, H.L. Frandsen, P.V. Hendriksen, Evaluation of thin film ceria membranes for syngas membrane reactors-Preparation, characterization and testing. Journal of Membrane Science, 378 (2011) 51-60.

[18] C. Chatzichristodoulou, M. Søgaard, J. Glasscock, A. Kaiser, S. Foghmoes, P.V. Hendriksen, Oxygen permeation in thin, dense $Ce_{0.9}Gd_{0.1}O_{1.95-\delta}$ membranes. Part II: Experimental determination. Journal of The Electrochemical Society, 158 (2011) F73-F83.

[19] A. Samson, M. Søgaard, R. Knibbe, N. Bonanos, High Performance Cathodes for Solid Oxide Fuel Cells Prepared by Infiltration of $La_{0.6}Sr_{0.4}CoO_{3-\delta}$ into Gd-Doped Ceria. Journal of The Electrochemical Society, 158 (2011) 1-10.

[20] J.M. Gozálvez-Zafrilla, A. Santafé-Moros, S. Escolástico, J.M. Serra, Fluid dynamic modeling of oxygen permeation through mixed ionic–electronic conducting membranes. Journal of Membrane Science 378 (2011) 290-300.

[21] C. Chatzichristodoulou, M. Søgaard, P.V. Hendriksen, Oxygen permeation in thin, dense $Ce_{0.9}Gd_{0.1}O_{1.95-\delta}$ membranes. Part I: Model study. Journal of The Electrochemical Society, 158 (2011) F61-F72.

[22] E. Girdauskaite, H. Ullmann, V.V. Vashook, U. Guth, G.B. Caraman, E. Bucher, W. Sitte, Oxygen transport properties of $Ba_{0.5}Sr_{0.5}Co_{0.8}Fe_{0.2}O_{3-\delta}$ and $Ca_{0.5}Sr_{0.5}Mn_{0.8}Fe_{0.2}O_{3-\delta}$ obtained from permeation and conductivity relaxation experiments. Solid State Ionics, 179 (2008) 385-392.

[23] W. Xie, H.F. Cheng, Z.Y. Chu, Z.H. Chen, Effect of carbonization time on the structure and electromagnetic parameters of porous-hollow carbon fibres. Ceramics International, 35 (2009) 2705-2710.

[24] C. Tablet, G. Grubert, H. Wang, T. Schiestel, M. Schroeder, B. Langanke, J. Caro, Oxygen permeation study of perovskite hollow fiber membranes. Catalysis Today, 104 (2005) 126-130.

[25] P. J. Gellings, H.J.M. Bouwmeester, Handbook of Solid State Electrochemistry CRC-Press 1996.

[26] A. Yan, B. Liu, Y. Dong, Z. Tian, D. Wang, M. Cheng, A temperature programmed desorption investigation on the interaction of $Ba_{0.5}Sr_{0.5}Co_{0.8}Fe_{0.2}O_{3-\delta}$ perovskite oxides with CO_2 in the absence and presence of H_2O and O_2. Applied Catalysis B: Environmental, 80 (2008) 24-31.

[27] V.B. Vert, J.M. Serra, Study of CO_2 stability and electrochemical oxygen activation of mixed conductors with low thermal expansion coefficient based on the $TbBaCo_3ZnO_{7+\delta}$ system. Journal of Power Sources, 196 (2011) 4270-4276.

FIGURE CAPTIONS

Figure 1. (a) Scheme of a cross section of the assembly thin film CGO membrane. (b) Schematic of the quartz membrane reactor design

Figure 2. SEM images of the fracture cross-section of the ceria membranes after the permeation test (a) CGO porous support; (b) CGO supported membrane (c) BSCF as catalytic coating (d) CeTbO+Co as catalytic coating

Figure 3. Dependence of the oxygen permeation flux through activated membranes on the sweep gas flow rate (Q_{Sweep}). (a) BSCF as catalytic coating, (b) CeTbO+Co as catalytic coating. Inset: corresponding variation of the oxygen flux as a function of pO_2 in the permeate.

Figure 4. The dependence of the oxygen permeation flux of a CGO supported membrane on the oxygen partial pressure difference on the air side (pO_2‘) and sweep side (pO_2“) at 950 ºC and 850 ºC. Argon is the sweep gas. (a) BSCF as catalytic coating; (b) CeTbO+Co as catalytic coating.

Figure 5. Oxygen permeation flux through activated membrane as a function of the temperature and oxygen partial pressure in the feed side. CeTbO+Co as catalytic coating; Argon as sweep gas; Q_{Sweep}=400 ml·min^{-1}; Q_{Feed}=100 ml·min^{-1}.

Figure 6. Oxygen permeation flux through activated membranes as a function of the temperature and air flow rate. Argon as sweep gas; Q_{Sweep}=400 ml·min^{-1}; pO_2‘=0.21 atm; (a) BSCF as catalytic coating; (b) CeTbO+Co as catalytic coating.

Figure 7. Oxygen permeation under methane feed as a function of the temperature. Q_{Sweep}=65 ml·min^{-1}; Q_{Feed}=60 ml·min^{-1}; synthetic air as feed (pO_2’=0.21 atm); CeTbO+Co as catalytic coating.

Figure 8. Temperature dependence of oxygen permeation flux through coated CGO supported membrane and the monolithic LSCF membrane. Performance after 48 h in CO_2 atmosphere at 750 ºC. Argon as sweep gas; Q_{Sweep}=65 ml·min^{-1}; Q_{Feed}=60 ml·min^{-1}; synthetic air as feed (pO_2’=0.21 atm); catalytic coating: CeTbO+Co.

Figure 9. Effect of the presence of CO_2 in the sweep gas. Temperature dependence of oxygen permeation flux through MIEC membranes. .Synthetic air as feed (pO_2’=0.21 atm), Q_{Feed}=60 ml·min^{-1}; sweep gas was Ar or a mixture Ar/CO_2 (85/15 vol.); Q_{Sweep}=65 ml·min^{-1}. (a) LSCF (b) activated CGO supported membrane; catalytic coating: CeTbO+Co.

Figure 10. Temperature dependence of oxygen permeation flux through activated membranes: effect of the pO_2 variation in the inlet sweep gas. Q_{Sweep}=400 ml·min^{-1},

Q_{Feed}=60 ml·min^{-1}; synthetic air as feed (pO_2'=0.21 atm); (a) BSCF as catalytic coating; (b) CeTbO+Co as catalytic coating.

Figure 1

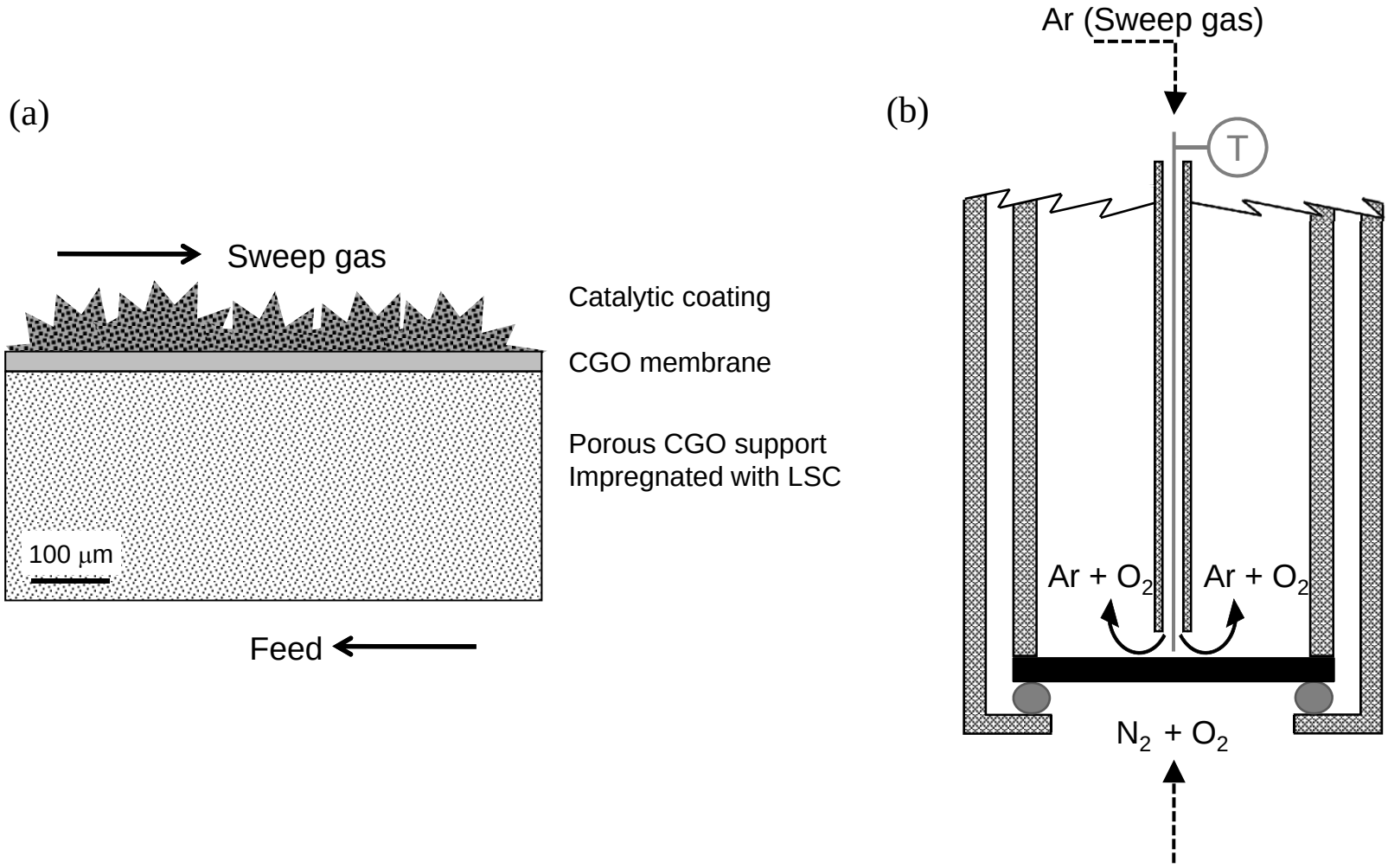

On the Use of Supported Ceria Membranes for Oxyfuel process / Syngas production

By *M. Pilar Lobera, José M. Serra, Søren P. Foghmoes, Martin Søgaard, Andreas Kaiser*

Figure 2

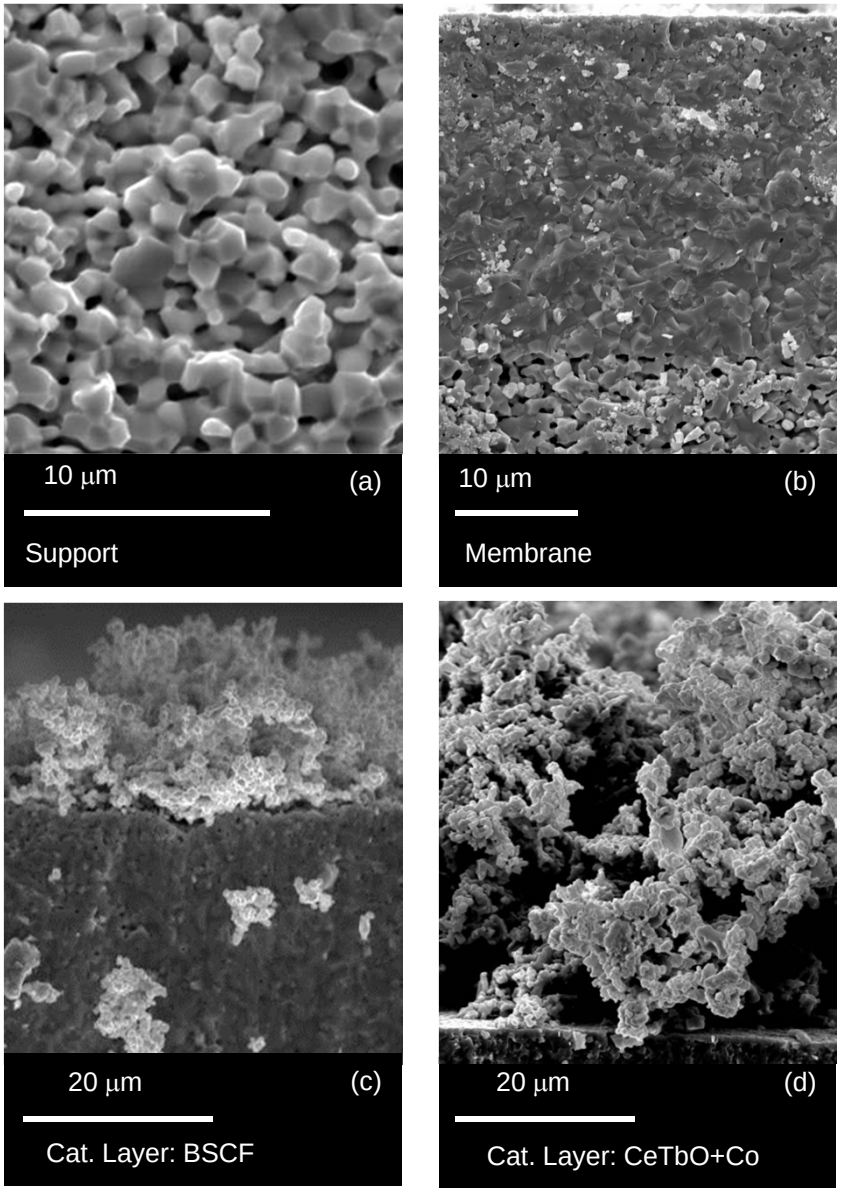

On the Use of Supported Ceria Membranes for Oxyfuel process / Syngas production
By *M. Pilar Lobera, José M. Serra, Søren P. Foghmoes, Martin Søgaard, Andreas Kaiser*

Figure 3

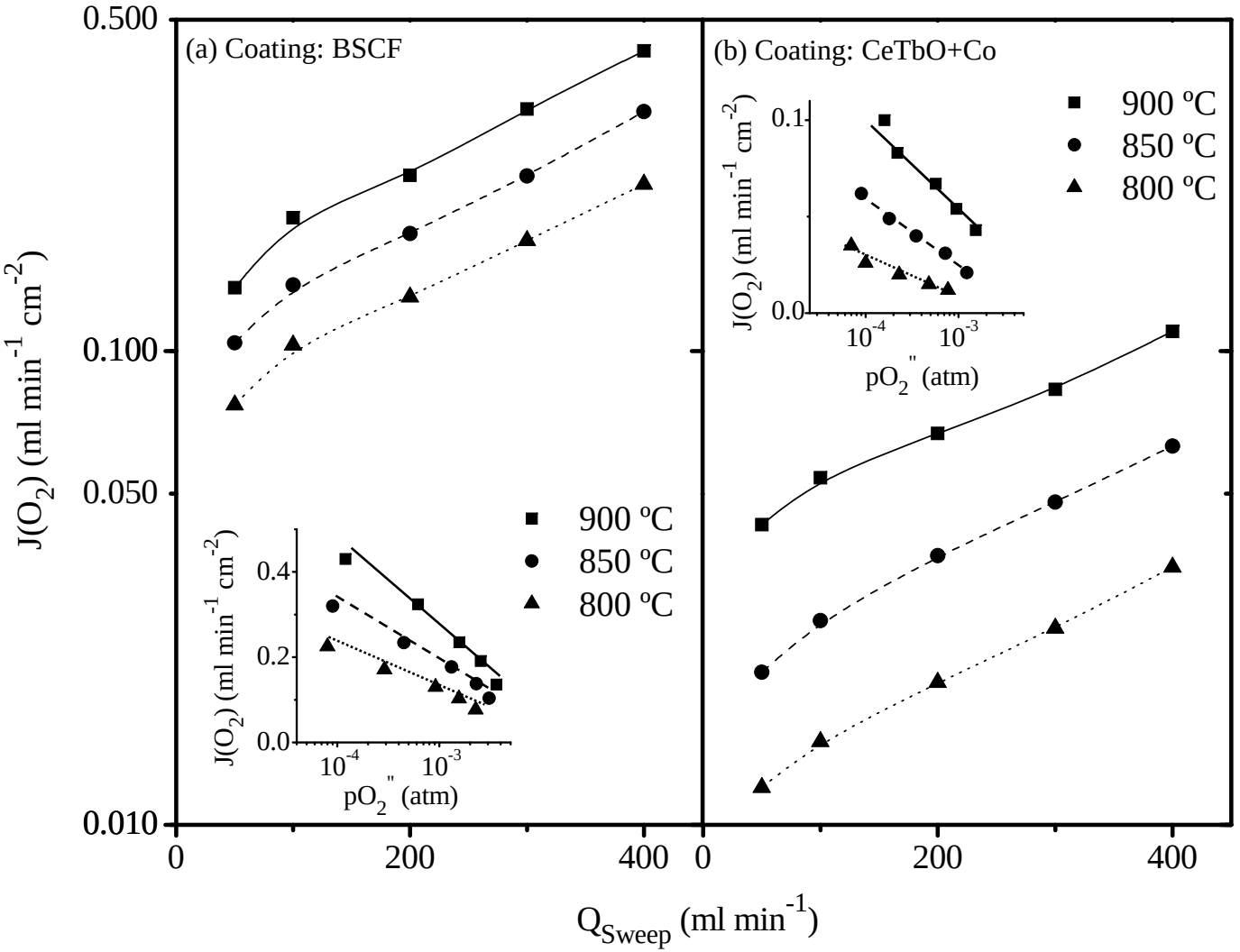

On the Use of Supported Ceria Membranes for Oxyfuel process / Syngas production

By *M. Pilar Lobera, José M. Serra, Søren P. Foghmoes, Martin Søgaard, Andreas Kaiser*

Figure 4

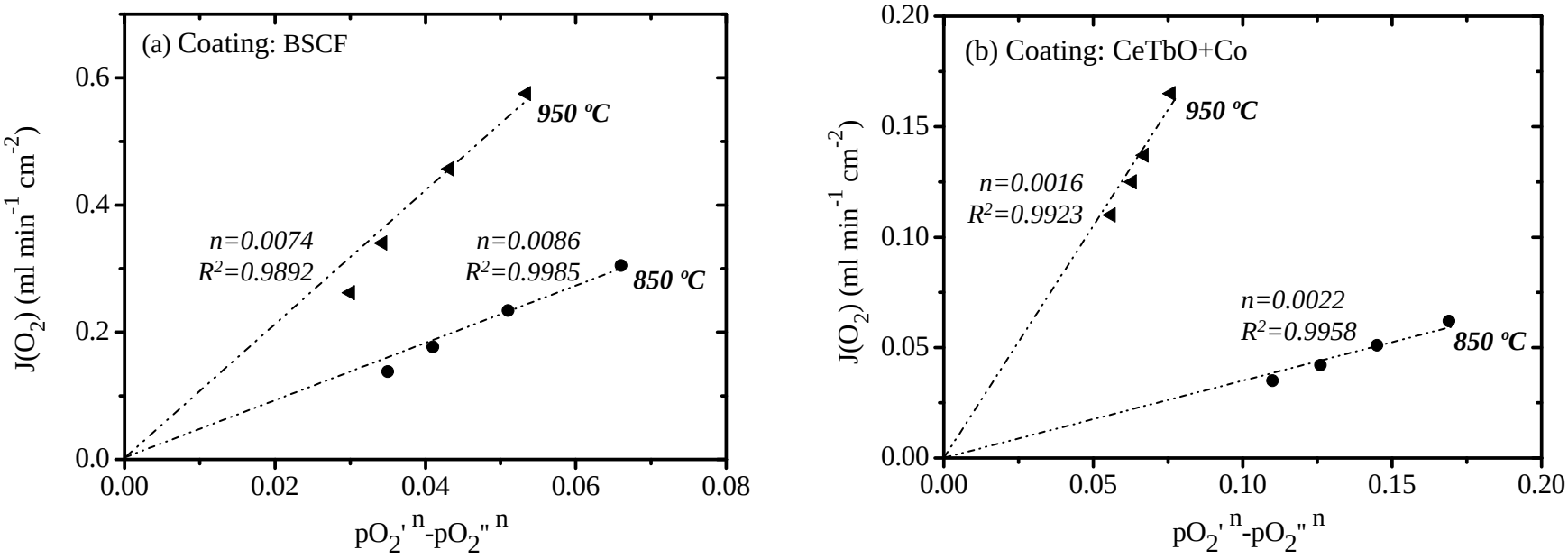

On the Use of Supported Ceria Membranes for Oxyfuel process / Syngas production
By *M. Pilar Lobera, José M. Serra, Søren P. Foghmoes, Martin Søgaard, Andreas Kaiser*

Figure 5

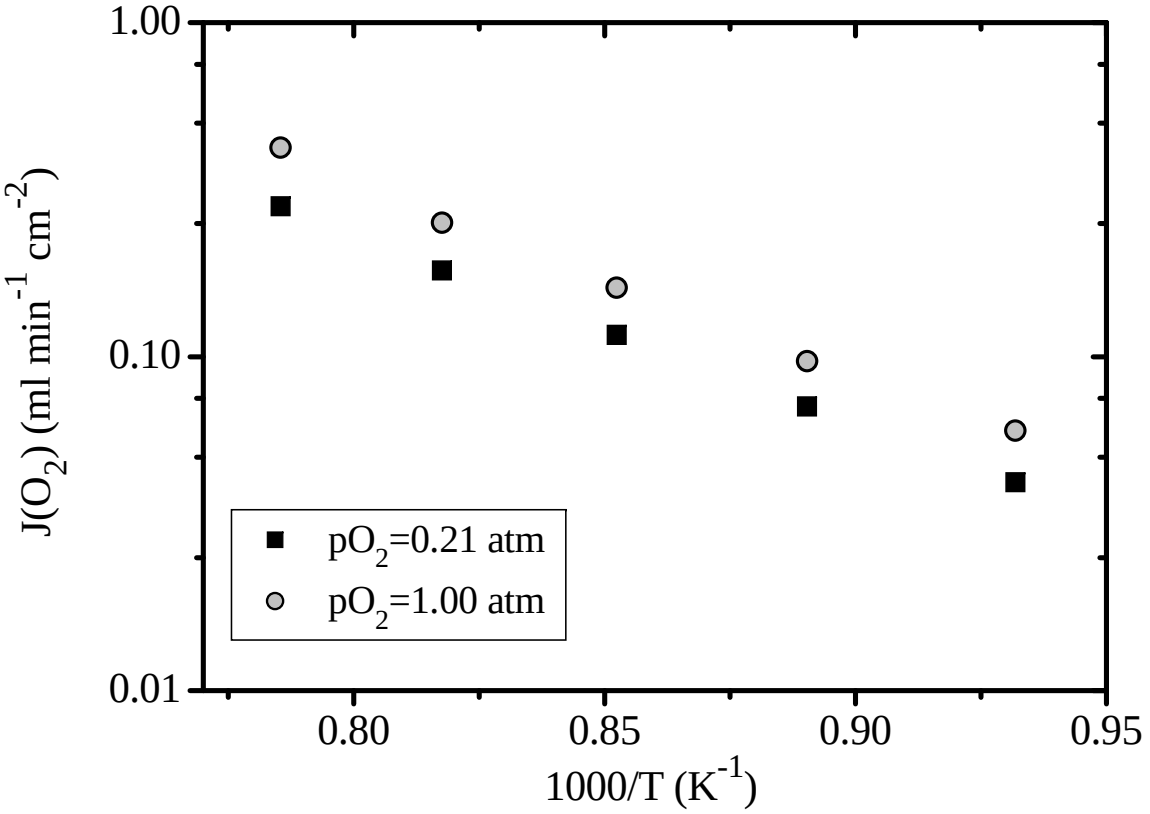

On the Use of Supported Ceria Membranes for Oxyfuel process / Syngas production
By *M. Pilar Lobera, José M. Serra, Søren P. Foghmoes, Martin Søgaard, Andreas Kaiser*

Figure 6

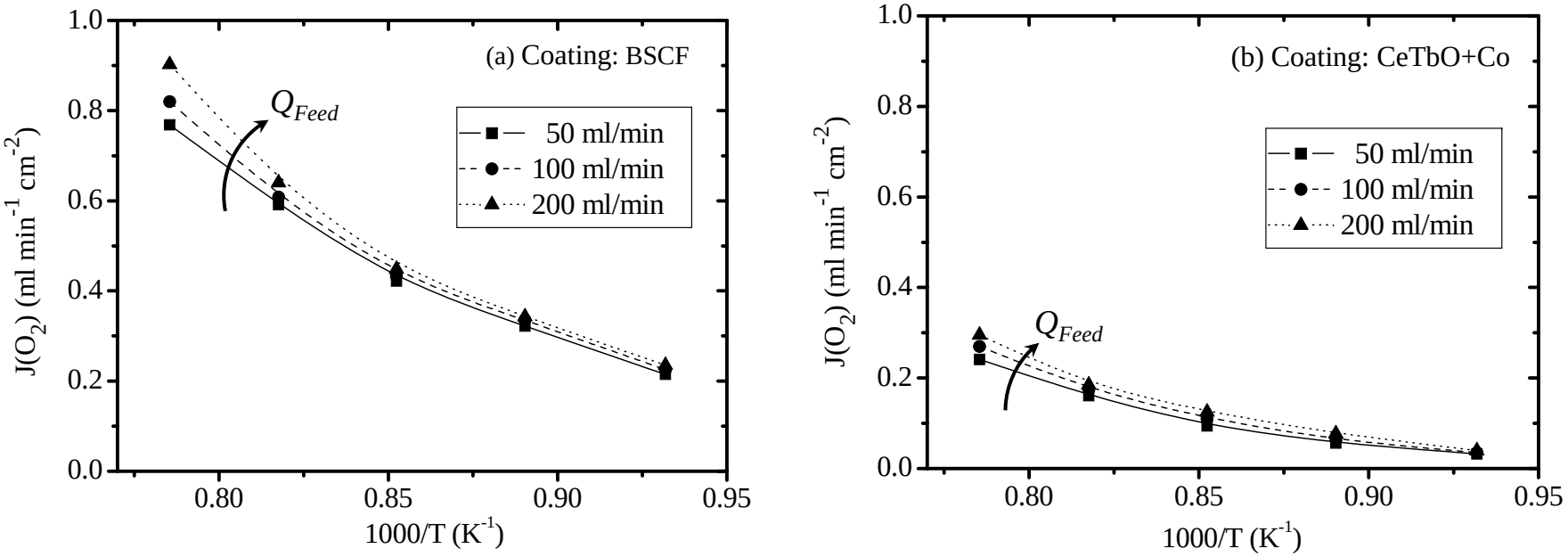

On the Use of Supported Ceria Membranes for Oxyfuel process / Syngas production
By *M. Pilar Lobera, José M. Serra, Søren P. Foghmoes, Martin Søgaard, Andreas Kaiser*

Figure 7

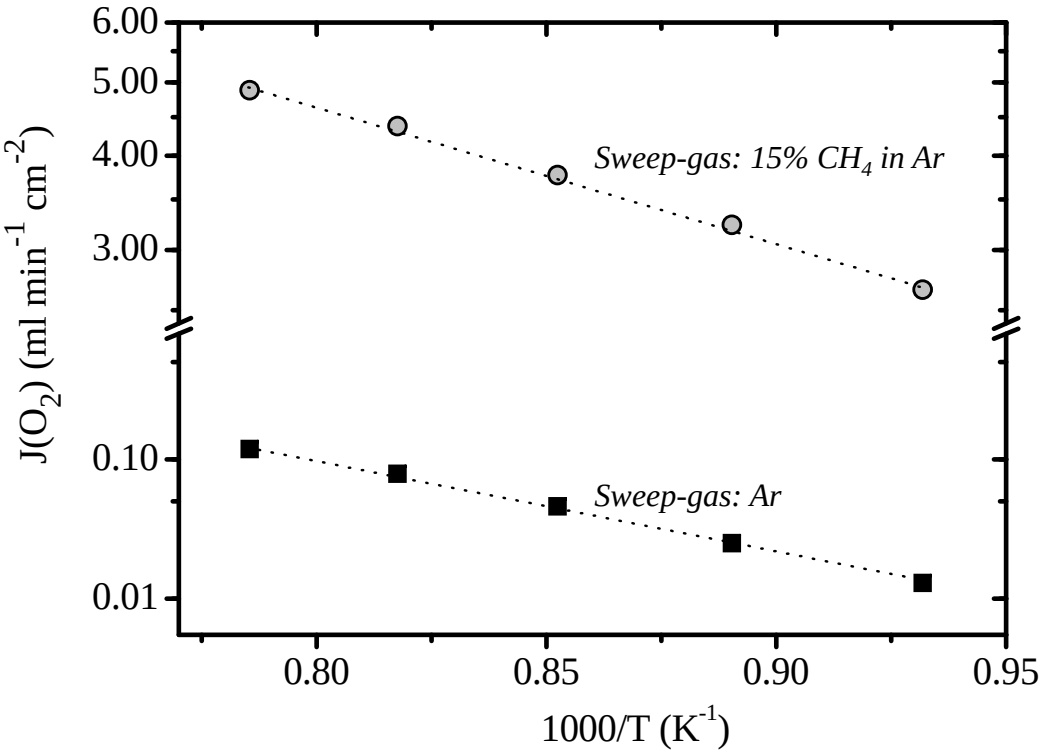

On the Use of Supported Ceria Membranes for Oxyfuel process / Syngas production
By *M. Pilar Lobera, José M. Serra, Søren P. Foghmoes, Martin Søgaard, Andreas Kaiser*

Figure 8

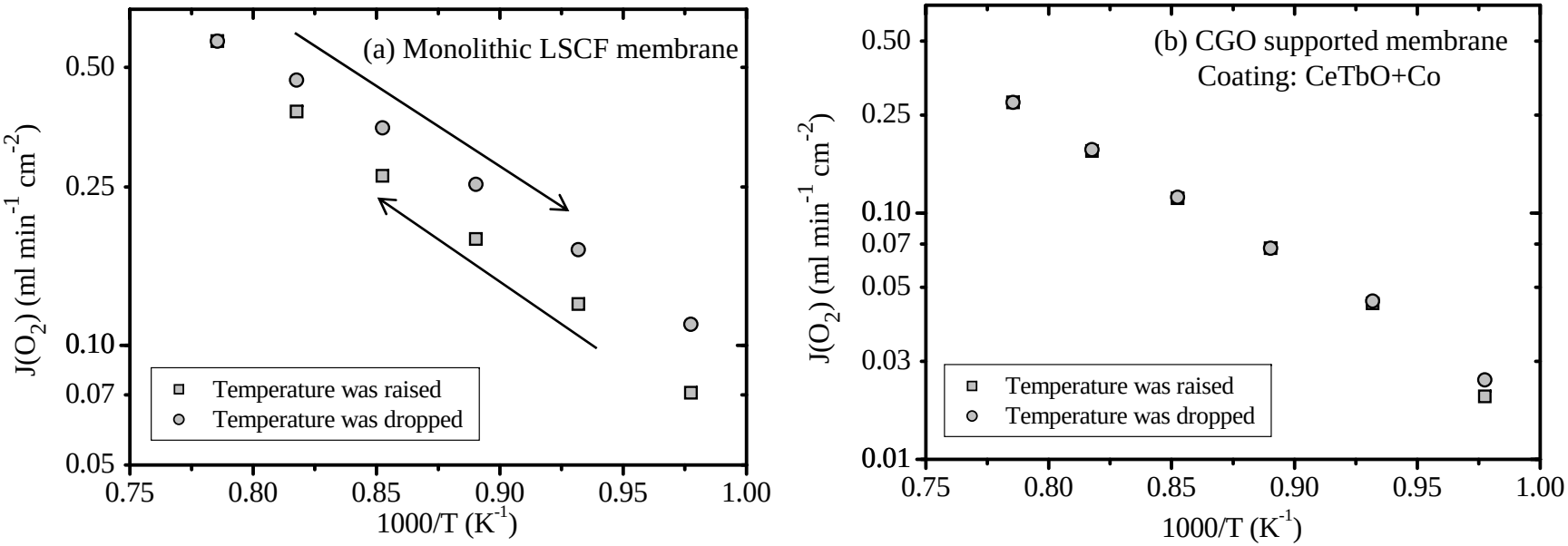

On the Use of Supported Ceria Membranes for Oxyfuel process / Syngas production

By *M. Pilar Lobera, José M. Serra, Søren P. Foghmoes, Martin Søgaard, Andreas Kaiser*

Figure 9

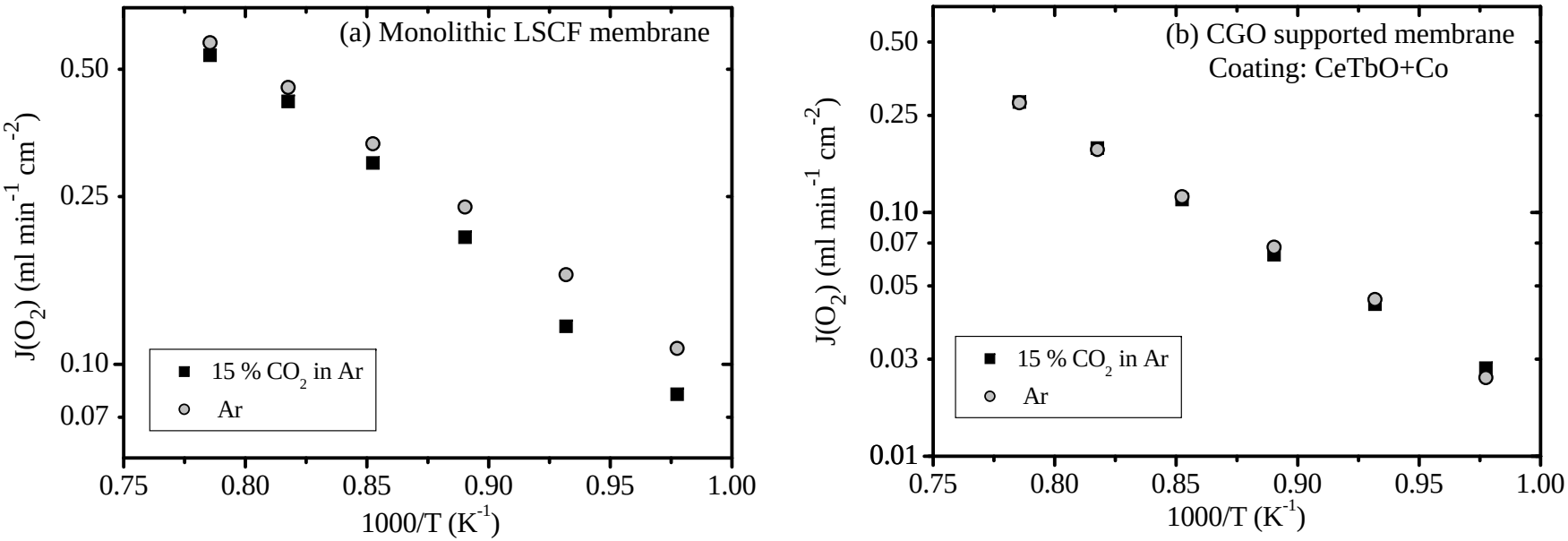

On the Use of Supported Ceria Membranes for Oxyfuel process / Syngas production

By *M. Pilar Lobera, José M. Serra, Søren P. Foghmoes, Martin Søgaard, Andreas Kaiser*

Figure 10

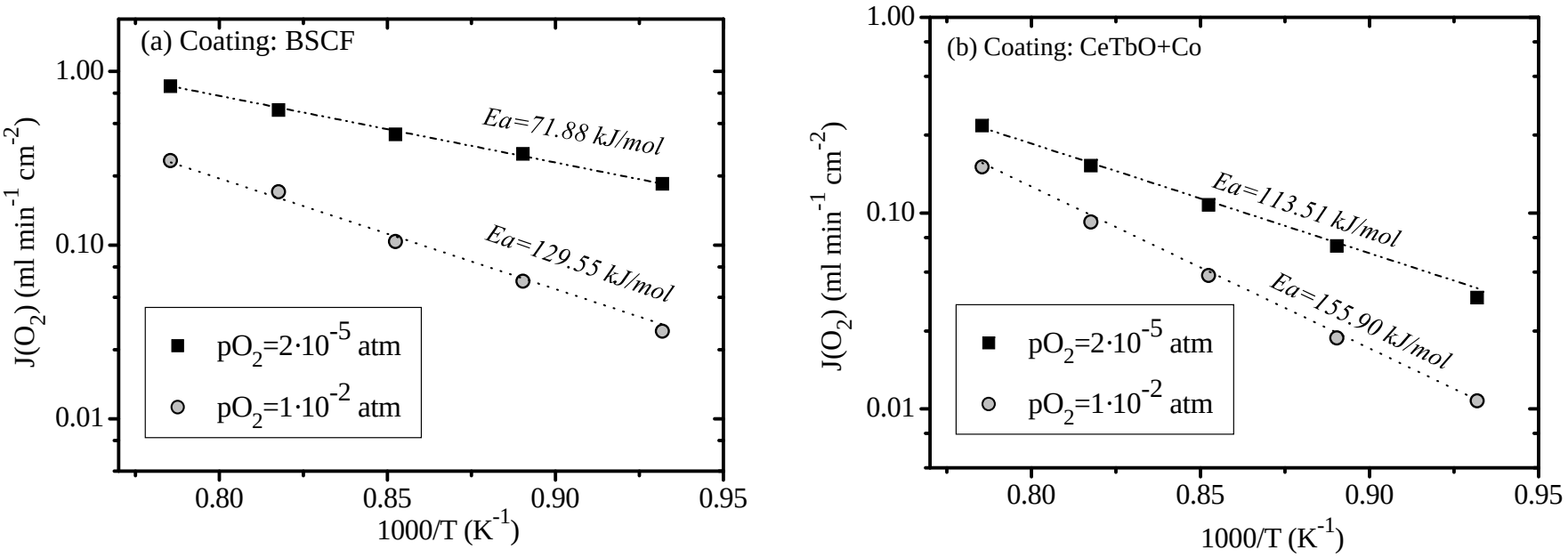

On the Use of Supported Ceria Membranes for Oxyfuel process / Syngas production

By *M. Pilar Lobera, José M. Serra, Søren P. Foghmoes, Martin Søgaard, Andreas Kaiser*

Supporting Information

From "On the Use of Supported Ceria Membranes for Oxyfuel process / Syngas production " by M. Pilar Lobera; José M. Serra; Martin Søgaard; Andreas Kaiser*

Figure S1

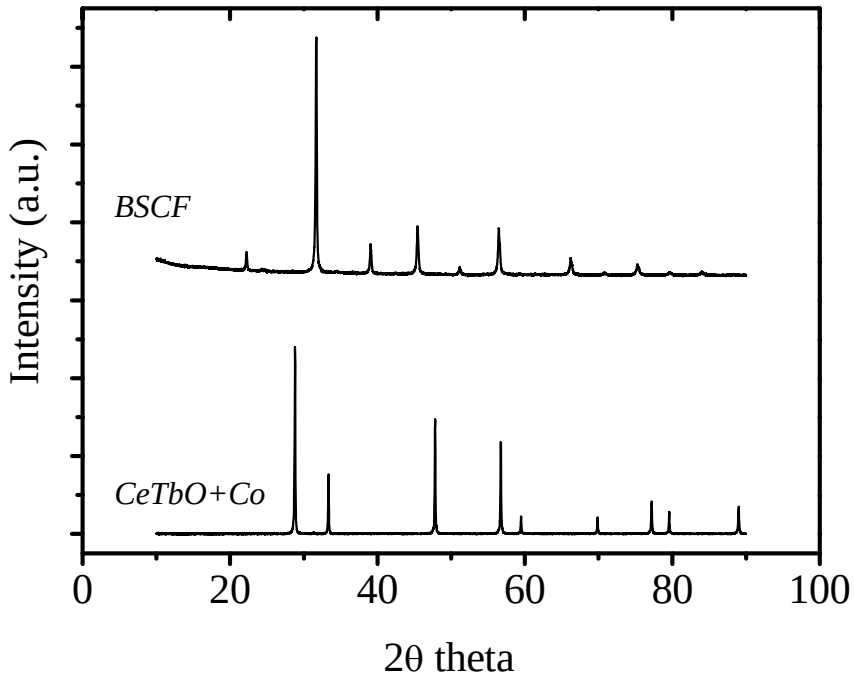

-.XRD paterns. $Ba_{0.5}Sr_{0.5}Co_{0.8}Fe_{0.2}O_{3-\delta}$ and $Ce_{0.8}Tb_{0.2}O_{2-\delta}$ + 2% Co mol powders after final sintered.-

Figure S2

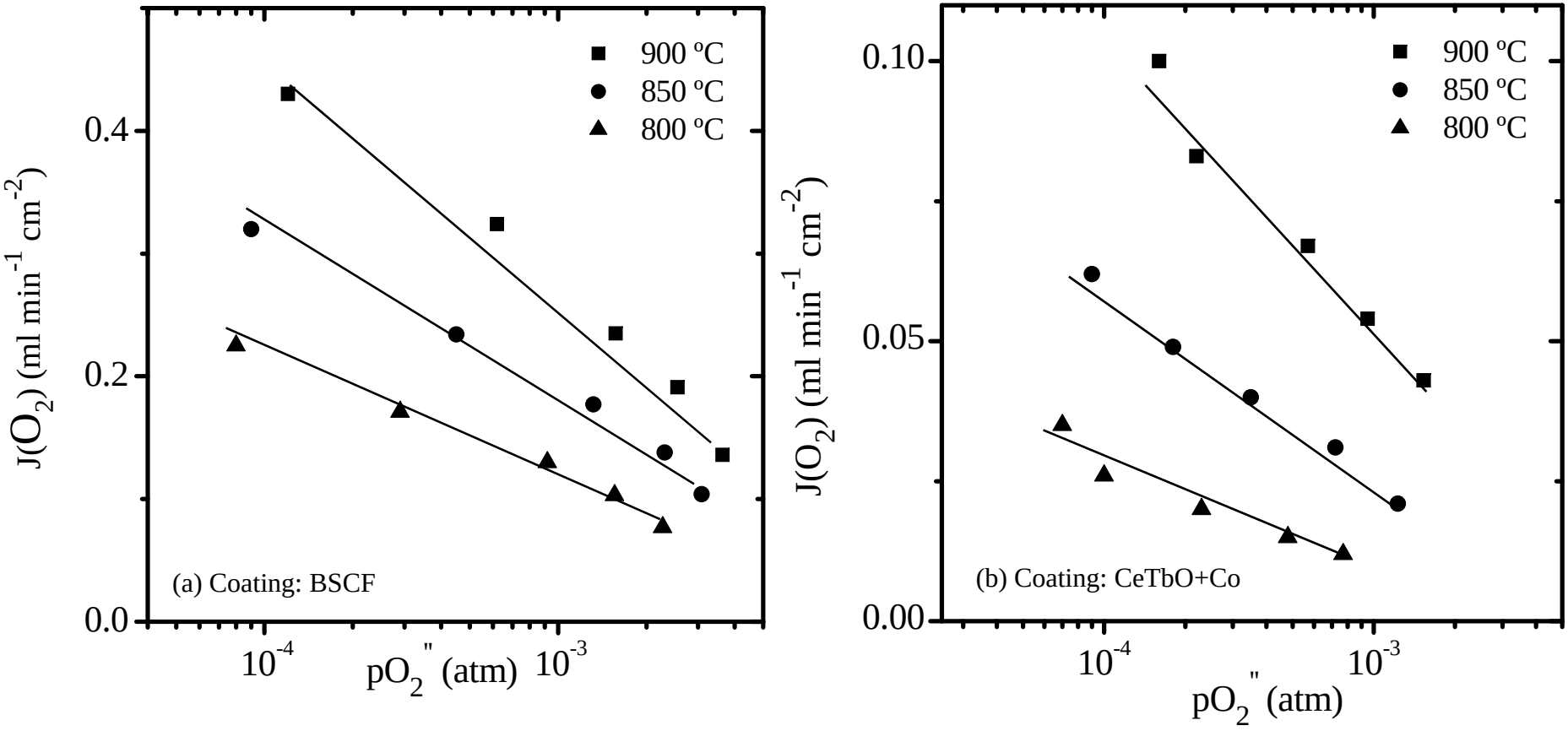

-. Dependence of the oxygen permeation flux through activated membranes as a function of pO_2 in the permeate; (a) BSCF as catalytic coating, (b) CeTbO+Co as catalytic coating.-

Figure S3

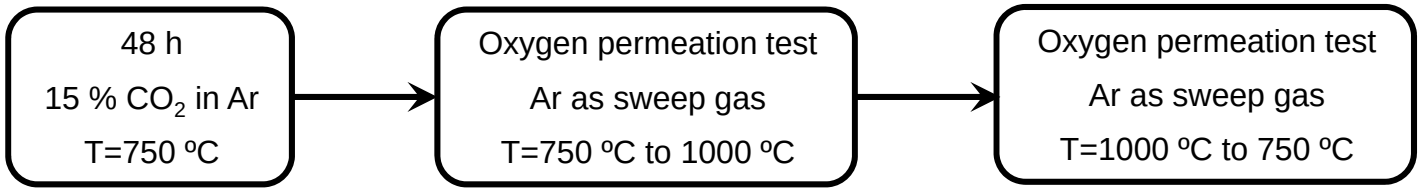

-. Experimental procedure for the CO_2 stability study, including a carbonation step and subsequent permeation test .-

Figure S4

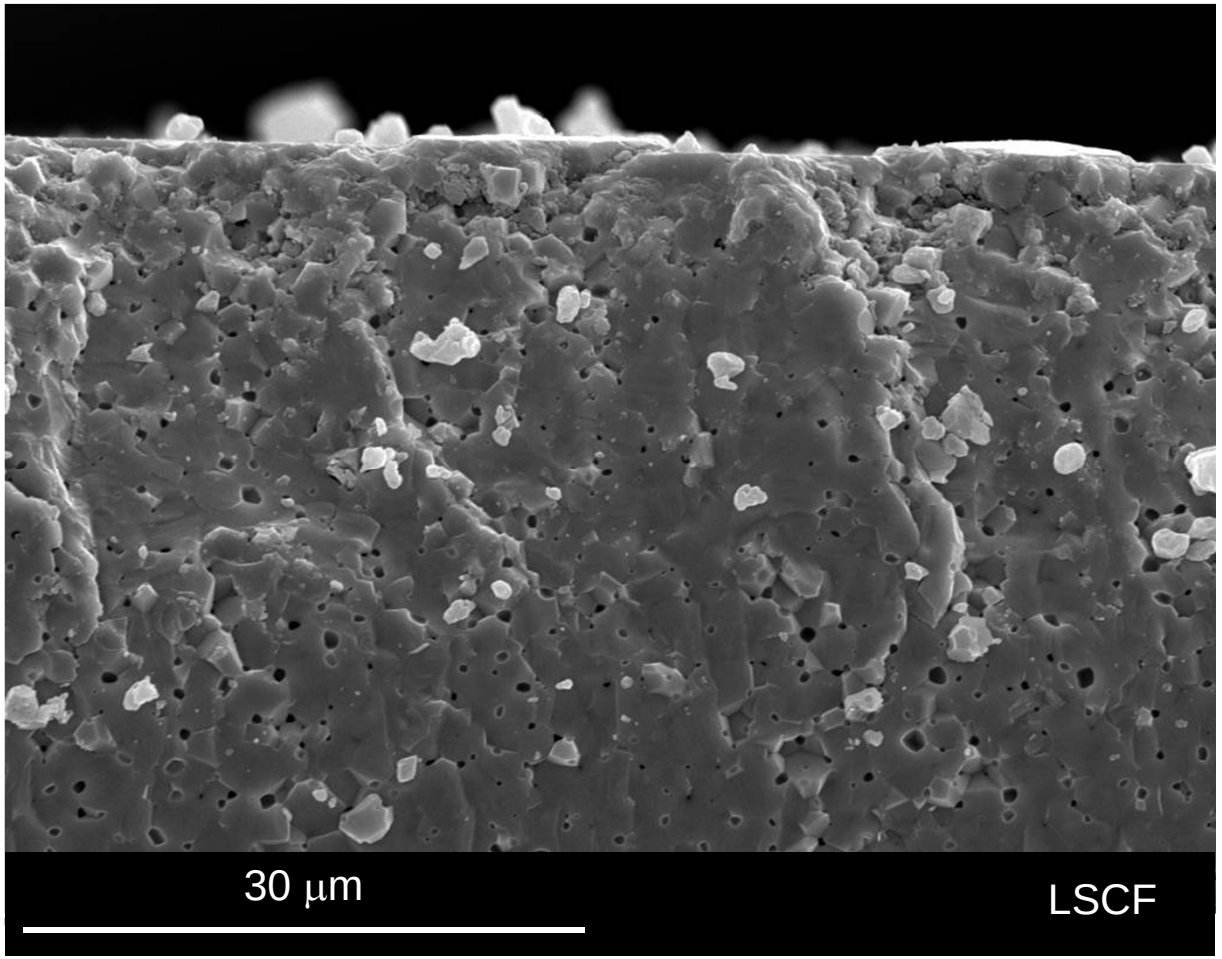

-. Postmortem SEM analysis of the fracture cross-section corresponding to the LSCF membranes, the top side is the side exposed to the sweep gas during the permeation testing.-